Research Article | Vol. 25, No. 20 | 2 Oct 2017 | OPTICS EXPRESS 23935
Optics EXPRESS

# Near-field edge fringes at sharp material boundaries

V. E. Babicheva,[1,2,4] S. Gamage,[1] M. I. Stockman,[1] and Y. Abate[1,3,5]

[1]*Center for Nano-Optics and Department of Physics and Astronomy, Georgia State University, P.O. Box 3965, Atlanta 30302, Georgia*
[2]*ITMO University, 49 Kronverksky Ave., St. Petersburg, 197101, Russia*
[3]*Department of Physics and Astronomy, University of Georgia, Athens 30602, Georgia*
[4]*baviev@gmail.com*
[5]*yabate@physast.uga.edu*

**Abstract:** We have studied the formation of near-field fringes when sharp edges of materials are imaged using scattering-type scanning near-field optical microscope (s-SNOM). The materials we have investigated include dielectrics, metals, a near-perfect conductor, and those that possess anisotropic permittivity and hyperbolic dispersion. For our theoretical analysis, we use a technique that combines full-wave numerical simulations of tip-sample near-field interaction and signal demodulation at higher orders akin to what is done in typical s-SNOM experiments. Unlike previous tip-sample interaction near-field models, our advanced technique allows simulation of the realistic tip and sample structure. Our analysis clarifies edge imaging of recently emerged layered materials such as hexagonal boron nitride and transition metal dichalcogenides (in particular, molybdenum disulfide), as well as traditional plasmonic materials such as gold. Hexagonal boron nitride is studied at several wavelengths, including the wavelength where it possesses excitation of phonon-polaritons and hyperbolic dispersion. Based on our results of s-SNOM imaging in different demodulation orders, we specify resonant and non-resonant types of edges and describe the edge fringes for each case. We clarify near-field edge-fringe formation at material sharp boundaries, both outside bright fringes and the low-contrast region at the edge, and elaborate on the necessity of separating them from propagating waves on the surface of polaritonic materials.



**OCIS codes:** (180.4243) Near-field microscopy; (310.6628) Subwavelength structures, nanostructures.

## References and links

1. Y. Abate, S. Gamage, L. Zhen, S. B. Cronin, H. Wang, V. Babicheva, M. H. Javani, and M. I. Stockman, "Nanoscopy reveals metallic black phosphorus," Light Sci. Appl. **5**(10), e16162 (2016).
2. S. Dai, Z. Fei, Q. Ma, A. S. Rodin, M. Wagner, A. S. McLeod, M. K. Liu, W. Gannett, W. Regan, K. Watanabe, T. Taniguchi, M. Thiemens, G. Dominguez, A. H. Castro Neto, A. Zettl, F. Keilmann, P. Jarillo-Herrero, M. M. Fogler, and D. N. Basov, "Tunable phonon polaritons in atomically thin van der waals crystals of boron nitride," Science **343**(6175), 1125–1129 (2014).
3. A. Woessner, M. B. Lundeberg, Y. Gao, A. Principi, P. Alonso-González, M. Carrega, K. Watanabe, T. Taniguchi, G. Vignale, M. Polini, J. Hone, R. Hillenbrand, and F. H. L. Koppens, "Highly confined low-loss plasmons in graphene-boron nitride heterostructures," Nat. Mater. **14**(4), 421–425 (2014).
4. S. Dai, Q. Ma, M. K. Liu, T. Andersen, Z. Fei, M. D. Goldflam, M. Wagner, K. Watanabe, T. Taniguchi, M. Thiemens, F. Keilmann, G. C. A. M. Janssen, S.-E. Zhu, P. Jarillo-Herrero, M. M. Fogler, and D. N. Basov, "Graphene on hexagonal boron nitride as a tunable hyperbolic metamaterial," Nat. Nanotechnol. **10**(8), 682–686 (2015).
5. A. Boulesbaa, V. E. Babicheva, K. Wang, I. I. Kravchenko, M.-W. Lin, M. Mahjouri-Samani, C. Jacob, A. A. Puretzky, K. Xiao, I. Ivanov, C. M. Rouleau, and D. B. Geohegan, "Ultrafast dynamics of metal plasmons induced by 2d semiconductor excitons in hybrid nanostructure arrays," ACS Photonics **3**(12), 2389–2395 (2016).
6. J. D. Caldwell, I. Vurgaftman, J. G. Tischler, O. J. Glembocki, J. C. Owrutsky, and T. L. Reinecke, "Atomic-scale photonic hybrids for mid-infrared and terahertz nanophotonics," Nat. Nanotechnol. **11**(1), 9–15 (2016).
7. P. Li, I. Dolado, F. J. Alfaro-Mozaz, A. Yu. Nikitin, F. Casanova, L. E. Hueso, S. Vélez, and R. Hillenbrand, "Optical Nanoimaging of Hyperbolic Surface Polaritons at the Edges of van der Waals Materials," Nano Lett. **17**(1), 228–235 (2017).
8. A. Poddubny, I. Iorsh, P. Belov, and Y. Kivshar, "Hyperbolic metamaterials," Nat. Photonics **7**(12), 948–957 (2013).

#301305 https://doi.org/10.1364/OE.25.023935
Journal © 2017 Received 29 Jun 2017; revised 31 Aug 2017; accepted 7 Sep 2017; published 21 Sep 2017

Optics EXPRESS


9. S. Ishii, A. V. Kildishev, E. Narimanov, V. M. Shalaev, and V. P. Drachev, "Sub-wavelength interference pattern from volume plasmon polaritons in a hyperbolic medium," Laser Photonics Rev. **7**(2), 265–271 (2013).
10. A. V. Chebykin, V. E. Babicheva, I. V. Iorsh, A. A. Orlov, P. A. Belov, and S. V. Zhukovsky, "Enhancement of the Purcell factor in multiperiodic hyperboliclike metamaterials," Phys. Rev. A **93**(3), 033855 (2016).
11. S. V. Zhukovsky, A. Orlov, V. E. Babicheva, A. V. Lavrinenko, and J. E. Sipe, "Photonic-band-gap engineering for volume plasmon polaritons in multiscale multilayer hyperbolic metamaterials," Phys. Rev. A **90**(1), 013801 (2014).
12. A. A. Orlov, A. K. Krylova, S. V. Zhukovsky, V. E. Babicheva, and P. A. Belov, "Multi-periodicity in plasmonic multilayers: general description and diversity of topologies," Phys. Rev. A **90**(1), 013812 (2014).
13. A. A. Orlov, E. A. Yankovskaya, S. V. Zhukovsky, V. E. Babicheva, I. V. Iorsh, and P. A. Belov, "Retrieval of Effective Parameters of Subwavelength Periodic Photonic Structures," Crystals **4**(3), 417–426 (2014).
14. Z. Jacob, I. I. Smolyaninov, and E. E. Narimanov, "Broadband Purcell effect: Radiative decay engineering with metamaterials," Appl. Phys. Lett. **100**(18), 181105 (2012).
15. Z. Jacob, J.-Y. Kim, G. V. Naik, A. Boltasseva, E. E. Narimanov, and V. M. Shalaev, "Engineering photonic density of states using metamaterials," Appl. Phys. B **100**(1), 215–218 (2010).
16. M. Y. Shalaginov, V. V. Vorobyov, J. Liu, M. Ferrera, A. V. Akimov, A. Lagutchev, A. N. Smolyaninov, V. V. Klimov, J. Irudayaraj, A. V. Kildishev, A. Boltasseva, and V. M. Shalaev, "Enhancement of single-photon emission from nitrogen-vacancy centers with TiN/(Al,Sc)N hyperbolic metamaterial," Laser Photonics Rev. **9**(1), 120–127 (2015).
17. M. A. K. Othman, C. Guclu, and F. Capolino, "Graphene-based tunable hyperbolic metamaterials and enhanced near-field absorption," Opt. Express **21**(6), 7614–7632 (2013).
18. C. Simovski, S. Maslovski, I. Nefedov, and S. Tretyakov, "Optimization of radiative heat transfer in hyperbolic metamaterials for thermophotovoltaic applications," Opt. Express **21**(12), 14988–15013 (2013).
19. K. L. Tsakmakidis, A. D. Boardman, and O. Hess, "Trapped rainbow' storage of light in metamaterials," Nature **450**(7168), 397–401 (2007).
20. V. E. Babicheva, M. Y. Shalaginov, S. Ishii, A. Boltasseva, and A. V. Kildishev, "Long-range plasmonic waveguides with hyperbolic cladding," Opt. Express **23**(24), 31109–31119 (2015).
21. V. E. Babicheva, M. Y. Shalaginov, S. Ishii, A. Boltasseva, and A. V. Kildishev, "Finite-width plasmonic waveguides with hyperbolic multilayer cladding," Opt. Express **23**(8), 9681–9689 (2015).
22. V. E. Babicheva, "Hyperbolic-metamaterial waveguides for long-range propagation," arxiv preprint arxiv:1707.07406 (2017).
23. S. Ishii, M. Y. Shalaginov, V. E. Babicheva, A. Boltasseva, and A. V. Kildishev, "Plasmonic waveguides cladded by hyperbolic metamaterials," Opt. Lett. **39**(16), 4663–4666 (2014).
24. V. E. Babicheva, "Multipole resonances and directional scattering by hyperbolic-media antennas," arXiv preprint arXiv:1706.07259 (2017).
25. Z. Jacob, L. V. Alekseyev, and E. Narimanov, "Optical hyperlens: far-field imaging beyond the diffraction limit," Opt. Express **14**(18), 8247–8256 (2006).
26. Z. Liu, H. Lee, Y. Xiong, C. Sun, and X. Zhang, "Far-field optical hyperlens magnifying sub-diffraction-limited objects," Science **315**(5819), 1686 (2007).
27. J. Sun, N. M. Litchinitser, and J. Zhou, "Indefinite by nature: from ultraviolet to terahertz," ACS Photonics **1**(4), 293–303 (2014).
28. T. Taubner, D. Korobkin, Y. Urzhumov, G. Shvets, and R. Hillenbrand, "Near-field microscopy through a SiC superlens," Science **313**(5793), 1595 (2006).
29. J. Chen, M. Badioli, P. Alonso-González, S. Thongrattanasiri, F. Huth, J. Osmond, M. Spasenović, A. Centeno, A. Pesquera, P. Godignon, A. Z. Elorza, N. Camara, F. J. García de Abajo, R. Hillenbrand, and F. H. Koppens, "Optical nano-imaging of gate-tunable graphene plasmons," Nature **487**(7405), 77–81 (2012).
30. Y. Abate, D. Seidlitz, A. Fali, S. Gamage, V. Babicheva, V. S. Yakovlev, M. I. Stockman, R. Collazo, D. Alden, and N. Dietz, "Nanoscopy of Phase separation in In1-xGaxN alloys," ACS Appl. Mater. Interfaces **8**(35), 23160–23166 (2016).
31. Y. Abate, V. E. Babicheva, V. S. Yakovlev, and N. Dietz, "Towards Understanding and Control of Nanoscale Phase Segregation in Indium-Gallium-Nitride Alloys," in *III-Nitride Materials, Devices, and Nano-Structures,*" Z. C. Feng, ed. (World Scientific Publishing, 2017), Chap. 6, pp. 183–207.
32. V. E. Babicheva, S. Gamage, L. Zhen, S. B. Cronin, V. S. Yakovlev, and Y. Abate, "Near-field Surface Waves in Few-Layer $MoS_2$," arxiv preprint arxiv:1707.07743 (2017).
33. Y. Abate, R. E. Marvel, J. I. Ziegler, S. Gamage, M. H. Javani, M. I. Stockman, and R. F. Haglund, "Control of plasmonic nanoantennas by reversible metal-insulator transition," Sci. Rep. **5**(1), 13997 (2015).
34. J. Zhu, K. Hippalgaonkar, S. Shen, K. Wang, Y. Abate, S. Lee, J. Wu, X. Yin, A. Majumdar, and X. Zhang, "Temperature-gated thermal rectifier for active heat flow control," Nano Lett. **14**(8), 4867–4872 (2014).
35. S. E. Grefe, D. Leiva, S. Mastel, S. D. Dhuey, S. Cabrini, P. J. Schuck, and Y. Abate, "Near-field spatial mapping of strongly interacting multiple plasmonic infrared antennas," Phys. Chem. Chem. Phys. **15**(43), 18944–18950 (2013).
36. S. Mastel, S. E. Grefe, G. B. Cross, A. Taber, S. Dhuey, S. Cabrini, P. J. Schuck, and Y. Abate, "Real-space mapping of nanoplasmonic hotspots via optical antenna-gap loading," Appl. Phys. Lett. **101**(13), 131102 (2012).

Optics EXPRESS

37. Z. Nuno, B. Hessler, B. Heiberg, R. Damato, T. Dunlap, Y. S. Shon, and Y. Abate, "Nanoscale near-field infrared spectroscopic imaging of silica-shell/gold-core and pure silica nanoparticles," J. Nanopart. Res. **14**(3), 766 (2012).
38. Z. Nuño, B. Hessler, J. Ochoa, Y. S. Shon, C. Bonney, and Y. Abate, "Nanoscale subsurface- and material-specific identification of single nanoparticles," Opt. Express **19**(21), 20865–20875 (2011).
39. J. M. Stiegler, Y. Abate, A. Cvitkovic, Y. E. Romanyuk, A. J. Huber, S. R. Leone, and R. Hillenbrand, "Nanoscale infrared absorption spectroscopy of individual nanoparticles enabled by scattering-type near-field microscopy," ACS Nano **5**(8), 6494–6499 (2011).
40. Y. Ogawa, F. Minami, Y. Abate, and S. R. Leone, "Nanometer-scale dielectric constant of Ge quantum dots using apertureless near-field scanning optical microscopy," Appl. Phys. Lett. **96**(6), 063107 (2010).
41. A. Cvitkovic, N. Ocelic, and R. Hillenbrand, "Material-specific infrared recognition of single sub-10 nm particles by substrate-enhanced scattering-type near-field microscopy," Nano Lett. **7**(10), 3177–3181 (2007).
42. B. Knoll and F. Keilmann, "Enhanced dielectric contrast in scattering-type scanning near-field optical microscopy," Opt. Commun. **182**(4-6), 321–328 (2000).
43. R. Hillenbrand, B. Knoll, and F. Keilmann, "Pure optical contrast in scattering-type scanning near-field microscopy," J. Microsc. **202**(P1), 77–83 (2001).
44. P. Li, M. Lewin, A. V. Kretinin, J. D. Caldwell, K. S. Novoselov, T. Taniguchi, K. Watanabe, F. Gaussmann, and T. Taubner, "Hyperbolic phonon-polaritons in boron nitride for near-field optical imaging and focusing," Nat. Commun. **6**, 7507 (2015).
45. S. Dai, Q. Ma, T. Andersen, A. S. Mcleod, Z. Fei, M. K. Liu, M. Wagner, K. Watanabe, T. Taniguchi, M. Thiemens, F. Keilmann, P. Jarillo-Herrero, M. M. Fogler, and D. N. Basov, "Subdiffractional focusing and guiding of polaritonic rays in a natural hyperbolic material," Nat. Commun. **6**, 6963 (2015).
46. *Scanning Probe Microscopy in Nanoscience and Nanotechnology*, B. Bhushan, ed. (Springer-Verlag Berlin Heidelberg, 2010).
47. L. J. Sherry, R. Jin, C. A. Mirkin, G. C. Schatz, and R. P. Van Duyne, "Localized surface plasmon resonance spectroscopy of single silver triangular nanoprisms," Nano Lett. **6**(9), 2060–2065 (2006).
48. D. Rossouw, M. Couillard, J. Vickery, E. Kumacheva, and G. A. Botton, "Multipolar plasmonic resonances in silver nanowire antennas imaged with a subnanometer electron probe," Nano Lett. **11**(4), 1499–1504 (2011).

## 1. Introduction

Recently emerged layered materials, such as black phosphorous, transition metal dichalcogenides (TMDCs), and hexagonal boron nitride (hBN), are promising for a wide range of applications in optoelectronics, and their optical properties at the nanoscale have generated enormous interest [1–7]. Hyperbolic metamaterials have recently attracted tremendous attention [8–13] due to potential applications in strong and broadband spontaneous emission and absorption enhancement [14–17], anomalous heat transfer [18], and slow light [19] as well as designs of waveguides [20–23], antennas [24], and hyperlenses [25,26]. However, most of the studies are related to artificially designed materials, so-called metamaterials, and most of the metamaterials have to incorporate metal elements which suffer high optical losses. Recently discovered layered materials with natural hyperbolic dispersion [27], such as hBN in the mid-infrared wavelength range [2], open up the possibility of designing devices with better functionality, e.g. less loss of the transmitted signal and higher optical resolution, and consequently may result in real-life applications. Scattering-type scanning near-field optical microscope (s-SNOM) has proved to be an important tool in optical characterizations of such material surfaces, providing direct real-space high-resolution images of surface states [28–42].

In s-SNOM experiments, near-field fringe formation at the sample edge is a rather complicated phenomenon for several reasons including but not limited to excitations of edge states and resonances in the structure, and multiple hot spots, as well as image artifacts due to feedback-related issues during rapid scanning around edges [43]. Theoretically, since the edge fringes are formed due to the complex interaction of a curved tip apex and sample, any reliable modeling should include a realistic tip size and shape. Simplified models that approximate the conical probe tip as a point dipole or spheroid [7] provide information about propagating surface waves on sample surfaces, but they cannot reproduce edge fringes that appear at the sample edge. Our work clarifies the origin of edge fringes in polarizable samples and plasmon or phonon resonant materials such as hBN that supports both bulk and surface hyperbolic waves [2,7,44,45].

Optics EXPRESS

Here, we study layered materials with different permittivities and demonstrate an approach to identify material types based on the s-SNOM image of sample edge. We develop a theoretical approach to predict and interpret s-SNOM results at different demodulation orders. When the tip is placed close to a sample surface and illuminated by a laser beam, a complex optical interaction between the tip and the sample takes place. Light is highly concentrated locally at the tip-sample junction (hot spot, Fig. 1), and the scattered field strongly depends on the gap size. The scattered signal depends on tip parameters (geometry and permittivity), sample properties, and the distance between the tip and the sample. We perform full-wave numerical simulations based on the finite-element method and take into account the tip-sample near-field interaction for any shape of the structure, not only flat surface, without any fitting parameters and not being restricted by semi-analytical point-dipole [42] or finite-dipole approximations [39].

We found that metal edges have pronounced bright fringes, whereas the edges of dielectrics do not show near-field edge fringes. Similar behavior is observed in layered van der Waals material hBN: bright edge fringes arise in the wavelength range where its dispersion is hyperbolic, and the fringes are absent at frequencies where the material is dielectric. Gold fringes in the visible range are affected by the plasmonic resonances near the edge, and we refer to it as *edge resonances*. These fringes are different from those in the mid-infrared range, where gold is a near-perfect conductor and does not support plasmonic resonances.

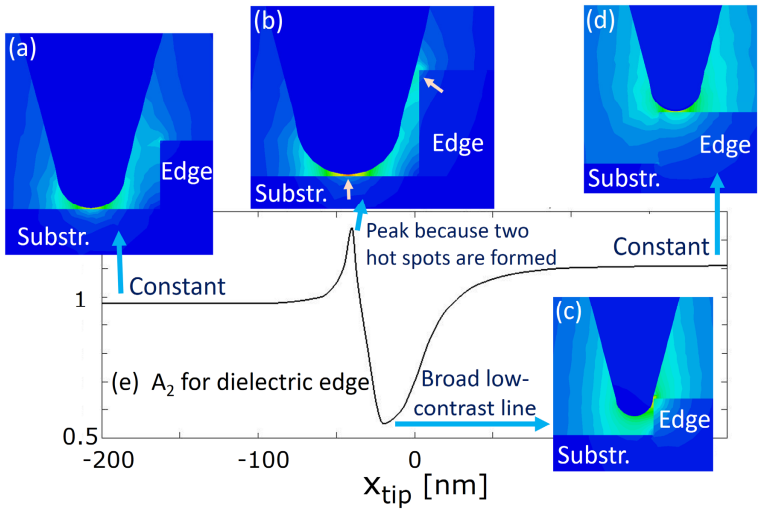


Fig. 1. Numerical calculations showing edge imaging in s-SNOM. (a)-(d) Various tip positions with respect to the dielectric edge and (e) line profile of calculated s-SNOM signal at 2nd harmonic ($A_2$) demodulation. In (b), $x_{tip} = -37$ nm ($x_{tip}$ is a position of the tip with respect to the edge), and two hot spots are formed: below the tip apex and at the edge; this results in the signal peak in (e). In (c) it is shown that the tip is displaced from the substrate below it and consequently does not couple to the substrate strongly, which results in the lower effective polarizability and the broad low-contrast line in the s-SNOM measurements.

## 2. Results and discussion

In our theoretical modeling, we consider a realistic conical shape of the tip illuminated by a plane electromagnetic wave. We account for the full structure, including the edge of the sample and the substrate, to realistically simulate the experiment. The tip is modeled as a truncated cone with the hemisphere at the tip apex (Fig. 1). The sphere radius is 30 nm, the cone base radius is 300 nm (which approximately corresponds to the total angle of 30°), and the cone height is 1 μm. We performed simulation tests with a smaller height, but only with 1 μm, the convergence of results has been achieved. The bulk part of the tip is silicon and the

Optics EXPRESS

surface is covered with 2-nm platinum, which closely resembles the tip used in our experiments.

We perform simulations of the full structure with the tip at different heights starting from 2 nm above the surface and assuming 60-nm oscillation amplitude. We then use the height-dependent reflectivity $r^{(\mathrm{CST})}(h)$ calculated by the CST Microwave Studio (frequency-domain solver) to evaluate the effective tip-sample polarizability $\alpha_{\mathrm{eff}}(h) = ia_1a_2(r^{(\mathrm{CST})}(h)) * \exp[-2ik_0\cos\theta(z_{\max} - z_{\mathrm{pos}})] \ /(2\pi k_0 \tan\theta)$, where $a_1$ and $a_2$ are the dimensions of the simulation box along the x- and y-axes, respectively (periodic boundary conditions are imposed), $k_0$ is the wave vector of the incident beam, θ is the angle of incidence, $z_{\max}$ is the upper boundary of the simulation box, and $z_{\mathrm{pos}}$ is the coordinate of the substrate surface. This approximation of effective polarizability is only applicable for p-polarized incident light, which is sufficient for most of the s-SNOM characterizations, and we use it throughout the paper. Calculations of effective polarizability for s-polarization requires taking into account different components of the tip polarizability tensor, and it is beyond the scope of the current work.

To extract the near-field response of the structure, it is essential to suppress contributions from other kinds of reflection and scattering that do not involve the near-field tip-sample interaction (e.g. reflection from tip shank and substrate). Therefore, the effective polarizability obtained in full-wave simulations is used to calculate the far-field radiation given by $E_{\mathrm{S}}(h_0 + \Delta h \sin\omega_{\mathrm{T}} t) = \sum_n s_n e^{in\omega_{\mathrm{T}} t}$, where $s_{\mathrm{n}}$ is the complex s-SNOM signal, $n$ is the demodulation order, and $\omega_{\mathrm{T}}$ is the natural frequency of the probe tip (typically on the order of 0.3 MHz). To simulate the experiments, we combine $E_{\mathrm{S}}$ with a reference field, $E_{\mathrm{M}}$, that is reflected from an oscillating mirror, implementing a pseudoheterodyne interferometer scheme. To reproduce the experimental measurements, we theoretically demodulate the normalized amplitude s-SNOM signal, which is extracted by dividing the signal at the sample by that at the substrate: $A_n = \left|s_{n,\mathrm{sample}}\right| / \left|s_{n,\mathrm{substrate}}\right|$

We perform full-wave simulations of the structure at different tip positions along the sample edge and calculate the signal in various demodulation orders. In combination with interferometric detection similar to the experiments, near-field signal free from background scattering is extracted from higher demodulation orders. At all demodulation orders, we observe a strong field enhancement at small tip-sample distances and a quickly decreasing signal as the tip moves away from the surface reproducing the experiments. Using our model, we analyze different materials and demodulation orders and investigate the formation of near-field edge fringes. In the near-field image of the edge, we specify two main features: a broad line of decreased signal and an outside bright fringe as described in more detail below.

First, we explain the low-contrast line that is formed at the edge of a material in s-SNOM images. A cantilevered tip vibrating at a near-resonance frequency is brought in close proximity to a sample surface. As the oscillating cantilever begins to approach the surface, the cantilever oscillation is reduced. The reduction in oscillation amplitude is used to identify and measure surface features [46], and a feedback loop maintains a constant tip-sample separation distance. In the theoretical model, we consider the tip oscillation amplitude of 60-nm and tip-sample distance of 2 nm at any closest point. When the probe tip approaches the edge of the structure, due to the curved profile of the tip, its apex does not couple to the substrate right beneath it [Fig. 1(c)]. The surrounding environment effectively possesses a smaller refractive index, so the effective polarizability of the tip is decreased; thus, a low-contrast line is formed in the s-SNOM image. Such low-contrast line is expected in s-SNOM images of the edge of materials that are sharp and thicker than a few tens of nanometers.

Second, we describe the outside bright fringe in non-resonant materials such as dielectrics and perfect electric conductors. When the tip scans the edge of a sharp sample boundary,

Optics EXPRESS

there is a point where two hot spots are formed: one at the substrate below the tip and one at the upper sharp edge of the sample, as shown in Fig. 1(b). The presence of two hot spots increases the scattered signal; consequently, the bright fringe is formed just outside the geometric edge of the sample. As the tip further moves away from the edge, only one hot spot – between the substrate and bottom of the tip – remains, and in the simulations, the s-SNOM signal in the substrate region is nearly independent of the tip position [Fig. 1(a)]. For the side hot spot, the tip-scattered field changes slower than for the hot spot formed below the tip.

In the mid-infrared wavelength range, gold produces strong near-field coupling with the probe tip, resulting in large s-SNOM amplitude contrast [Fig. 2(a)]. In this range, optical properties of the gold are similar to the properties of the perfect electric conductor: the real part of the permittivity is negative, while the absolute values of real and imaginary parts of the permittivity are large, so the skin depth is extremely small. Because of this, no plasmonic resonances are involved, the outside bright fringe corresponds to the position of the tip where two hot spots are formed, and the fringe weakens at higher demodulation orders of s-SNOM measurements. Thus, gold edge in the mid-infrared range is non-resonant.

Edge fringes depend on the direction of light incidence, but in the case of the incidence perpendicular to the edge, the profiles are very similar whether the light comes from the substrate or from the sample side (not shown here). In contrast, beam propagating along the edge results in stronger fringes with more sophisticated features [Fig. 2(b)]. In any case, the outside bright fringe corresponds to two hot spots, and the low-contrast line is present.

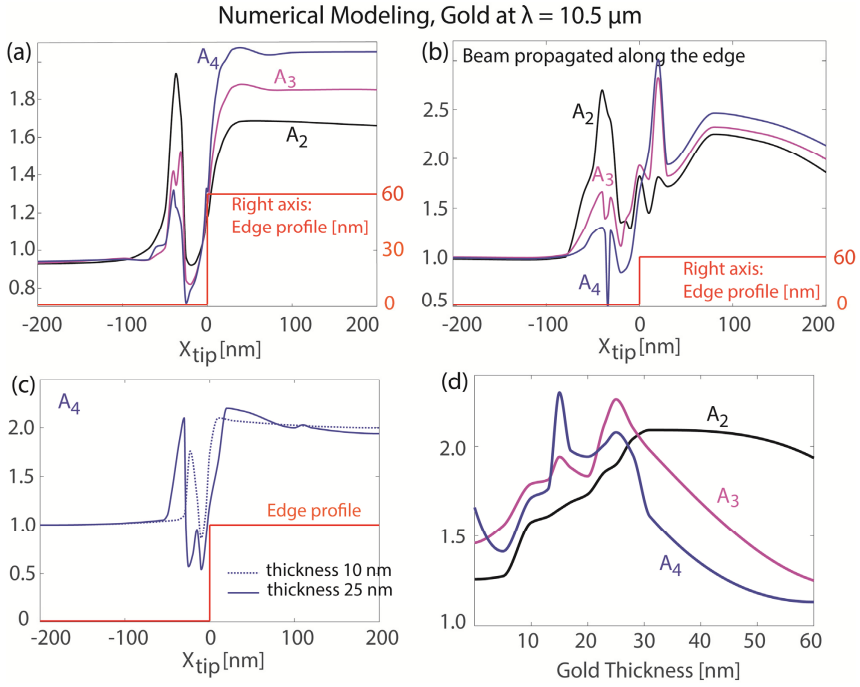


Fig. 2. Numerical calculations for gold in the mid-infrared range where its properties are similar to the perfect electric conductor. (a) Change of contrast in different demodulation orders $A_n$ in the case of beam incident perpendicular to the edge. Gold thickness is 60 nm. The signal is normalized so that it is equal to 1 on the substrate at the distance 2 μm in each demodulation order. At the tip position $x_{tip}$ = –200 nm, the edge slightly affects the signal, which results in a small deviation from 1. (b) The same as (a) but for the beam propagating along the edge. (c) Change of contrast $A_4$ for thicknesses of the gold 10 and 25 nm. (d) Change of contrast for different gold thickness at the point of two-hot-spot formation. The change of contrast does not reach 1 for the layers of several nanometers as the highly reflective boundary affects the signal.

Optics EXPRESS

The sample edge height and the tip shape define the position $x_{tip}$ where two hot spots are simultaneously formed. For gold films with thickness down to 10 nm, the simulations predict both outside bright fringe and low-contrast line [Fig. 2(c)], however, their experimental observation may be hindered by sample/tip imperfections. Ultimately, in the experiment, the s-SNOM resolution is limited by the tip apex size, and observation of the smaller features in either dimension is difficult. Furthermore, the gold edge is highly reflective, but for other non-resonant materials with moderate permittivity, direct experimental imaging of the fringe is difficult due to weak signal. In Fig. 2(d) we show theoretical values of $A_n$ at the fringe peak for samples with different thicknesses. The peak position changes with the change of layer thickness and dip in the profiles become closer as the film thickness decreases [Fig. 2(c)]. The calculated signal strength also shows strong demodulation-order dependence.

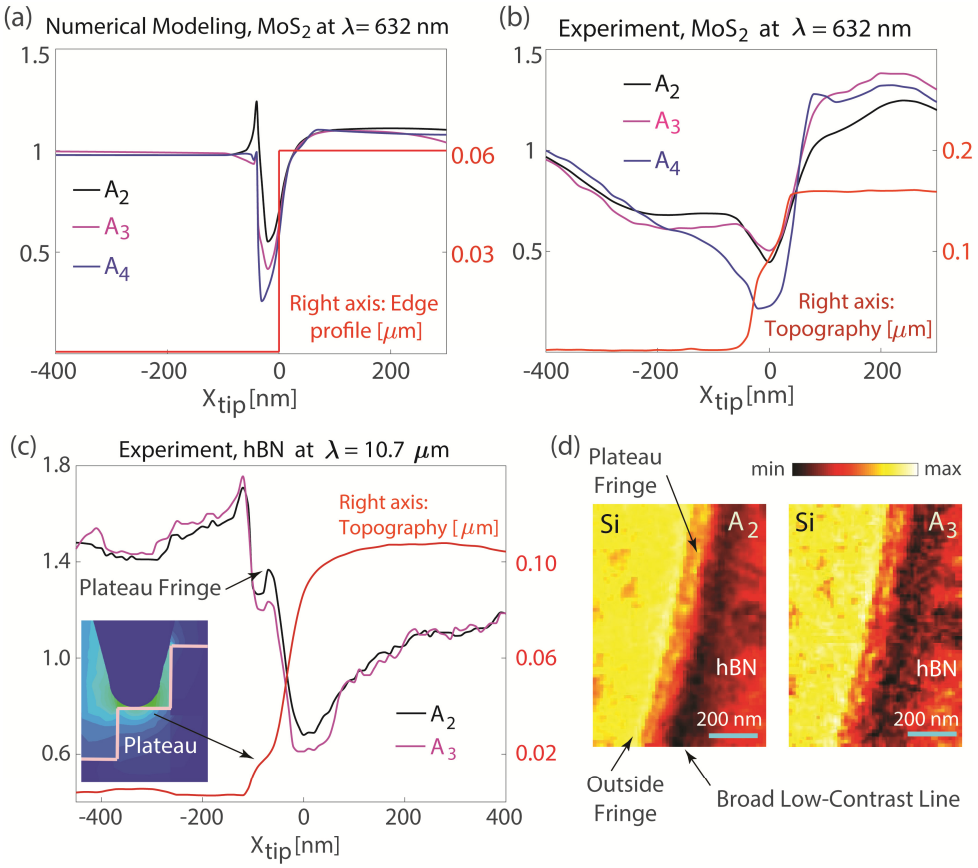


Fig. 3. Edge fringes in materials at different harmonics of the tip resonance frequency $(A_{\text{norm}})_n$. (a) and (b) Numerical modeling and experimental images, respectively, for an $MoS_2$ (dielectric) on silicon at λ = 632 nm. (c) Line profiles taken from s-SNOM near-field images and (d) s-SNOM amplitude images for hBN on silicon at the laser wavelength, λ = 10.7 μm, where hBN is an anisotropic dielectric. The sample edge has a plateau, which results in an additional outside plateau fringe.

Similar to gold, at higher demodulation orders, the bright fringe at the edge of dielectric materials weakens [Figs. 3(a) and 3(b)]. Exfoliable materials usually have very sharp edges, and the outside fringes are more pronounced in comparison to the edges of other materials with similar permittivity. For thick exfoliable materials (thickness > ~50 nm), the edge may have several plateaus, which are clearly seen in the topography line profile [Fig. 3(c)]. The presence of plateaus could result in multiple outside fringes, as shown in the experimental

Optics EXPRESS

near-field amplitude images of hBN on silicon at $\lambda = 10.7$ μm [Figs. 3(c) and 3(d)] where hBN is an anisotropic dielectric.

For materials with plasmonic properties or with hyperbolic dispersion, the tip excites edge, and the efficiency of the excitations changes with the tip position. This results in pronounced changes in the scattered near-fields. The origin of the edge resonances can be any resonance in the structure where the resonance is largely defined by the distribution of the fields near the edge. We demonstrate edge resonances for a plasmonic metal (gold in the visible wavelength range) and hBN at a mid-infrared wavelength, a material with a hyperbolic dispersion that supports phonon-polaritons and their multiple reflections within the layer.

For resonant materials, the brightest point at the edge may appear somewhere in the intermediate position of the tip [as shown in Fig. 1(c)]. This is especially pronounced for hBN with hyperbolic dispersion [Figs. 4(c) and 4(d)]. In particular, we consider the excitation wavelength $\lambda = 7$ μm, where hBN permittivity components are ($\varepsilon_{\text{in-plane}} = -14.6 + 1i$ and $\varepsilon_{\text{out-of-plane}} = 2.7 + 0.0004i$), which results in the hyperbolic dispersion. Out-of-plane component of the permittivity tensor is relatively small, and consequently, no fringe is observed related to two hot spots for hyperbolic hBN. The bright fringes in hBN s-SNOM images are related to the most efficient excitation of hyperbolic phonon-polaritons and resonant reflection of the ray in the layer (Fig. 4(a) [44,45],). The direction of the rays is defined by the tensor components of the permittivity (see analytical expressions in [10,44,45]) and thus the strongest excitation occurs only at the particular position of the tip with respect to the edge.

Plasmonic materials, such as gold in the visible wavelength range, have a more complex fringe profile with two peaks [Figs. 4(e) and 4(f)]. The peak for negative $x_{\text{tip}}$ corresponds to two-hot-spot excitation and strong light reflection from them. The second peak results from an efficient excitation of plasmonic edge resonances. This resonance is similar to other plasmonic excitations that occur in nanostructures, where the permittivity of metal is comparable with permittivity of surrounding dielectrics [47,48]. However, our theory model does not provide accurate results for this case as the model is limited by the dipole approximation of the tip scattering and does not account for higher multipoles, which can be important in the case of plasmonic nanostructures of complex shape.

A number of reasons may cause smearing out the outside bright fringe. First of all, if the edge is not sharp and layer thickness decreases gradually having plateaus, the main peak is smaller and additional peaks appear at the plateaus, which is observed in Fig. 3 and most likely explains the discrepancy of numerical modeling and experimental results. In addition, the condition of the tip used in the experiments does not necessarily match the simulation tip parameters. Second, as we have shown, an increase of layer thickness results in non-monotonic changes in all demodulation orders. For instance, in the case of gold, third and fourth demodulation orders have maximum values for the thickness of several tens of nanometers, which can be attributed to the most efficient coupling of near fields at two hot spots [Fig. 2(d)]. For relatively thick samples, two hot spots are further away from each other, they are less coupled, and resulting bright fringe is weaker. Also, for such thick structures, the peak of the bright fringe becomes further away from the edge, it is more affected by the variations in the tip shape, and the outside bright fringe will be smeared out [2].

## 3. Conclusion

We have extensively investigated the formation of near-field edge fringes that arise at sharp material edges in s-SNOM measurements. The edge fringes are distinct from other fringes that appear at the sample surface because of the propagation of surface and bulk waves and can give information on the strength of material polarizability as well as on their plasmon or phonon resonance edge properties.

Optics EXPRESS

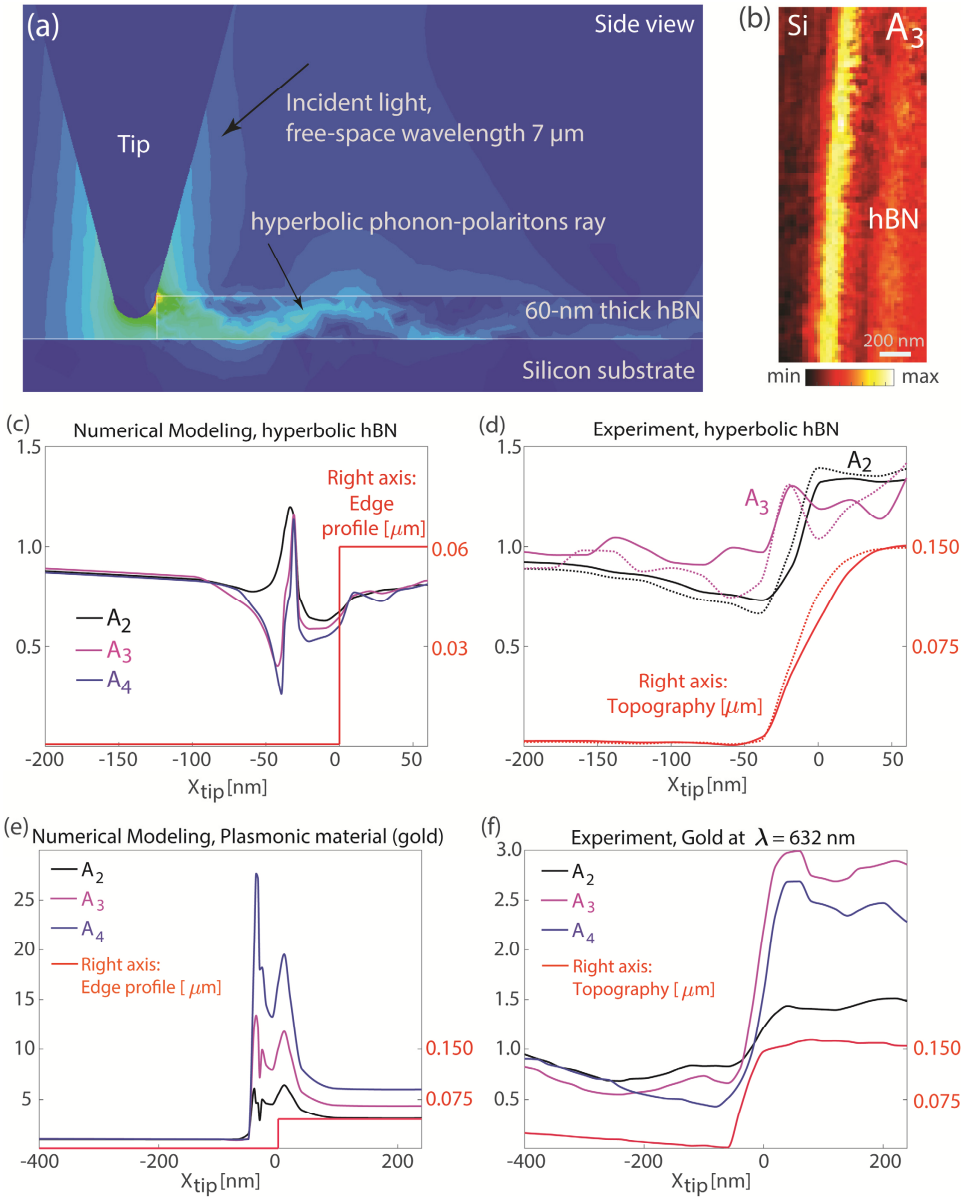


Fig. 4. Edge fringes in plasmonic or phononic structures. (a) Schematic side view of a cross-section of the edge characterization of hBN sample and propagation of deeply subwavelength phonon-polariton rays in 60-nm-thick layer excited by the light with λ = 7 μm. The most efficient excitation and pronounced outside bright fringe occur at the intermediate position of the tip in respect to the sample edge: $x_{tip}$ = –31 nm, which in the numerical simulations corresponds to the peaks in the signal ($A_3$ and $A_4$) of hBN edge characterization. (b) s-SNOM image of hBN at the 3rd harmonic of the tip frequency ($A_3$). hBN fringes in the hyperbolic regime at λ = 7 μm are different from the fringes of dielectric hBN at λ = 10.7 μm [see Figs. 3(c) and 3(d)]. (c) Numerical modeling and (d) experimental results of the change of contrast in different demodulation orders $A_n$ for hBN that has a hyperbolic dispersion at λ = 7 μm ($\varepsilon_{in\text{-}plane}$ = –14.6 + 1i and $\varepsilon_{out\text{-}of\text{-}plane}$ = 2.7 + 0.0004i). The peak of the signal occurs at $x_{tip}$ = –31 nm [panel (c)], which means it is offset from the point where two hot spots are created simultaneously (tip/edge and tip/substrate at $x_{tip}$ = –37 nm). In panel (d), the solid and dotted lines correspond to two experimental measurements, and they agree remarkably well. (e) Numerical modeling and (f) experimental results respectively for plasmonic material: at λ = 632 nm, gold permittivity is ε = –12 + 1.3i, and plasmonic edge resonances are excited.

Optics EXPRESS

## 4. Method

The microscope is a commercial s-SNOM system (neaspec.com). A probing linearly *p*-polarized QCL laser is focused on the tip–sample interface at an angle of 45° to the sample surface. The scattered field is acquired using a phase modulation (pseudoheterodyne) interferometry. The background signal is suppressed by vertical tip oscillations at the mechanical resonance frequency of the cantilever ($f_0$ ~285 kHz) and demodulation of the detector signal at higher harmonics $nf_0$, $n$ = 2, 3, 4, of the tip resonance frequency. The combined scattered field from the tip and the reference beam pass through a linear polarizer, which further selects the p/p polarization of the measured signal for analysis.

## Funding

National Science Foundation (553251); Air Force Office of Scientific Research (AFOSR) (FA9559-16-1-0172); Materials Sciences and Engineering Division of the Office of the Basic Energy Sciences, Office of Science, U.S. Department of Energy (DE-SC0007043).

## Acknowledgment

SG and YA acknowledge support by the National Science Foundation under grant no. 1553251. The work of VEB is supported by the Air Force Office of Scientific Research (AFOSR) grant number FA9559-16-1-0172. MIS acknowledges support from the Materials Sciences and Engineering Division of the Office of the Basic Energy Sciences, Office of Science, U.S. Department of Energy, Grant No. DE-SC0007043.

The authors acknowledge fruitful discussions with Vladislav Yakovlev.